buildings

MDPI

Article

Displacement and Internal Force Response of Mechanically Connected Precast Piles Subjected to Horizontal Load Based on the m-Method

Li Gao [1,2], Mei-Ling Zhuang [3,4,*], Qunqun Zhang [5], Guangdong Bao [4], Xiaoyang Yu [4], Jiahao Du [4], Shengbo Zhou [1,2] and Mingsen Wang [3]

[1] School of Civil Engineering and Architecture, Suqian University, Suqian 223800, China; gaoli@squ.edu.cn (L.G.); zhoushengbo2005@163.com (S.Z.)
[2] Jiangsu Province Engineering Research Center of Prefabricated Building and Intelligent Construction, Suqian University, Suqian 223800, China
[3] Water Resources Research Institute of Shandong Province, Jinan 250013, China; wang_ms88@163.com
[4] School of Transportation and Civil Engineering, Nantong University, Nantong 226019, China; 18051133608@163.com (G.B.); 15050658281@163.com (X.Y.); 15093016704@163.com (J.D.)
[5] School of Transportation and Civil Engineering, Anhui Jianzhu University, Hefei 23061, China; 15532395385@163.com
* Correspondence: ml_zhuang@ntu.edu.cn or ml_zhuang99@163.com

Abstract: Mechanically connected precast piles are a type of precast piles that utilise snap-type mechanical connectors to restrain the pile ends of two identical or different precast piles at the top and bottom so as to quickly realise the purpose of the connection. However, the gap problem in the connectors of mechanically connected piles can lead to uneven and uniform deformation of the piles under horizontal loading, resulting in additional displacements and rotation angles of the piles at the connection. Solving the problem of calculating the internal force response of discontinuous deformed piles is a prerequisite for promoting and applying mechanically connected precast piles. Firstly, the theoretical derivation of mechanically connected piles with fixed constraints at the pile bottom is carried out. Secondly, the pile response equations of mechanically connected piles are established, and the theoretical solutions of pile displacement and internal force response of mechanically connected piles under horizontal loading are derived. Thirdly, the pile-soil model of the test pile is established using ABAQUS software (ABAQUS 2016) in combination with the design data of the test pile. The numerical simulation displacements and angles of rotation are compared with the test results. Finally, the theoretical and numerical simulation displacements and internal forces of the ordinary pile and the mechanically connected pile are compared. The relative errors of the displacements and angles of rotation of the established pile-soil model are less than 10%, indicating that the established model has good accuracy. The relative errors of the theoretical and numerical simulation displacements and internal forces of the mechanically connected pile are less than 10%, proving the correctness of the theoretical calculation by the m-method. This study can provide effective theoretical support and methodological guidance for the displacement and internal force response of discontinuous piles.

Keywords: prestressed solid square piles; mechanically connected piles; m-method; displacement curve equations; soil-pile model

check for updates

Citation: Gao, L.; Zhuang, M.-L.; Zhang, Q.; Bao, G.; Yu, X.; Du, J.; Zhou, S.; Wang, M. Displacement and Internal Force Response of Mechanically Connected Precast Piles Subjected to Horizontal Load Based on the m-Method. *Buildings* **2024**, *14*, 1943. https://doi.org/10.3390/buildings14071943

Academic Editor: Eugeniusz Koda

Received: 25 April 2024
Revised: 19 June 2024
Accepted: 21 June 2024
Published: 26 June 2024

Copyright: © 2024 by the authors. Licensee MDPI, Basel, Switzerland. This article is an open access article distributed under the terms and conditions of the Creative Commons Attribution (CC BY) license (https://creativecommons.org/licenses/by/4.0/).

1. Introduction

A pile foundation is one of the most widely used forms of upper load bearing in various deep foundation categories in actual projects. It can adapt to various sizes of loads, various directions of distribution, and various complex geological conditions. It also has the advantages of large bearing capacity, high stability, relatively small settlement value, and good durability under the condition of well-treated foundations. Therefore,

pile foundations have been widely used in construction fields such as roads and bridges, super-high-rise buildings, and major projects such as harbour terminals [1–3].

Among the commonly used pile foundations, bored piles are the most widely used [4], but they require on-site pouring construction, which has the disadvantages of high construction noise, serious environmental pollution and a long construction period, which is no longer in line with the development prospect of industrialisation, information technology, and greening of China's construction industry, and thus has limitations in the process of its use. While precast structures [5,6] are produced in factory workshops, the environmental pollution of on-site construction can be effectively controlled, which has a high application prospect. At present, welding is still the main method for connecting prefabricated piles, such as square piles and tubular piles. However, the welding process, though simple, is demanding and often cannot be effectively implemented at construction sites, resulting in inconsistent welding quality. During the piling process, any defects in the joint welds are magnified, making the joints the weak points of the piles. Among prefabricated pile foundation project quality accidents, the accidents caused by the quality of joint welding accounted for a large proportion.

Mechanically connected precast piles are an improved type of precast piles using snap-in mechanical connectors (see Figure 1a), which can confine the pile ends of two identical or different precast piles (see Figure 1b) at the top and bottom to quickly realize the purpose of connection [7–9]. Compared with ordinary precast square piles, the connection process of mechanically connected piles does not require welding, and the connection effect can be achieved by extruding and butt jointing, which have the advantages of high efficiency, environmental protection and reliability [10,11]. In addition, due to the replaceability of mechanically connected piles, the precast piles have a wider range of combinations of pile lengths, cross-sections, and reinforcement ratios, which improves the fault tolerance of precast pile production.



(**a**) (**b**)

Figure 1. Photos of prestressed solid square piles and a nap-type mechanical connector. (**a**) Prestressed solid square piles. (**b**) A snap-in mechanical connector.

Under the action of horizontal external load, the precast pile will undergo bending deformation, and the soil body also squeezes reaction force on the pile body [12]. Therefore, the response of the pile under horizontal loading mainly involves the joint bearing of the pile body and soil body to the external load. Different soil conditions and depths of entry can greatly affect the internal force response generated by the pile. Different theoretical methods have been proposed for the displacement and internal force response of pile foundations under horizontal action [13]. Among the widely used theoretical methods, the main ones are the ultimate foundation reaction method, the elastic foundation reaction method and the elastoplastic foundation reaction method. The elastic foundation reaction force method is a method based on Winkler's elastic foundation beam model [14]. It regards the pile as an elastic beam and considers the magnitude of the reaction force per unit length of the foundation beam to be proportional to the settlement of the foundation beam of that length. Then, according to the force relationship between the pile and foundation

soil when they act together, the differential equations are established to be solved by the m-method [15,16]. For the horizontal load response of ordinary piles, researchers have jointly discussed the feasibility of the m-method in the horizontal load response of piles through theoretical analysis, numerical simulations and experimental studies and put forward a series of problems and suggestions [17,18]. Our latest public bridge regulations issued in 2019 [19] provided a detailed and systematic introduction to the calculation of horizontal displacement and action effects of elastic piles by the m-method, proposing a weight conversion method for the equivalent m-value of the scale factor for multi-storey foundations and a correction method for the maximum bending moment of the pile. García et al. [20] performed horizontal load tests on near-true scale foundation models of defective and intact three-pile systems. On the basis of the experimental data, a preliminary calibration of the 3D finite element analysis was carried out, which was subsequently used to investigate the effect of defective elements on the pile load distribution and the horizontal base force at the pile shaft. The results indicated that the presence of a defective pile increased the raft tilting, which affected vertical and horizontal load distributions among the raft and the piles, as well as among tailing and leading piles.

The problem of gaps in the connectors of mechanically connected piles can lead to uneven and uniform deformation of the pile under horizontal loading, which in turn leads to additional displacement and rotation angles of the piles at the connection. Solving the problem of calculating the internal force response of discontinuous deformed piles is a prerequisite for the popularisation and application of mechanically connected precast piles. Firstly, the theoretical derivation of mechanically connected piles with fixed constraints at the pile bottom is carried out. Secondly, the pile response equations of mechanically connected piles are established, and the theoretical solutions of pile displacement and internal force response of mechanically connected piles under horizontal load are derived. Thirdly, the pile-soil model of the test pile from reference [21] is established using ABAQUS software. The numerical simulation results of the pile-soil model are compared with the test results to verify the correctness of the pile-soil model. Finally, the theoretical and numerical simulation displacement and internal forces of the ordinary pile and mechanically connected pile are compared to verify the correctness of the theoretical calculation by the m-method.

2. Theoretical Calculation of Displacement and Internal Force Response of Mechanically Connected Piles

2.1. Description of Stress Phases and Basic Assumptions

Under horizontal loading, the deformation of the pile body after the mechanically connected pile is subjected to force is not as uniform as that of ordinary tubular piles, and an additional structural angle of rotation will be generated at the connection due to the existence of a gap in the mechanical connection. The physical drawing and conceptual drawing of the angle of rotation diagram of the mechanically connected pile structure are shown in Figure 2a,b.

The following assumptions are made based on the stressing process and state of mechanically connected piles. The assumptions are made as follows.

(1) Upper pile stress stage.

When the load is small and acts on the top of the upper pile, the top of the pile first undergoes a displacement and an angle of rotation when the horizontal external load acts on the top of the connected pile. Due to the structural angle of rotation φ, it is assumed that the bottom connection of the upper pile undergoes only rotation without horizontal displacement, i.e., the connection is considered as an equivalent plastic hinge, while the lower pile is considered as fixed and unresponsive.

(2) Critical state

The horizontal load continues to increase until the structural rotation angle reaches the limit value of the structural angle of rotation φ_0. The structural angle of rotation reaches

the limit value, meaning that the simple upper pile force reaches the critical state, and the combined effect of the external loads in the critical state is solved by the boundary condition of the state, which is used as the basis for judgement of the connecting pile force state.

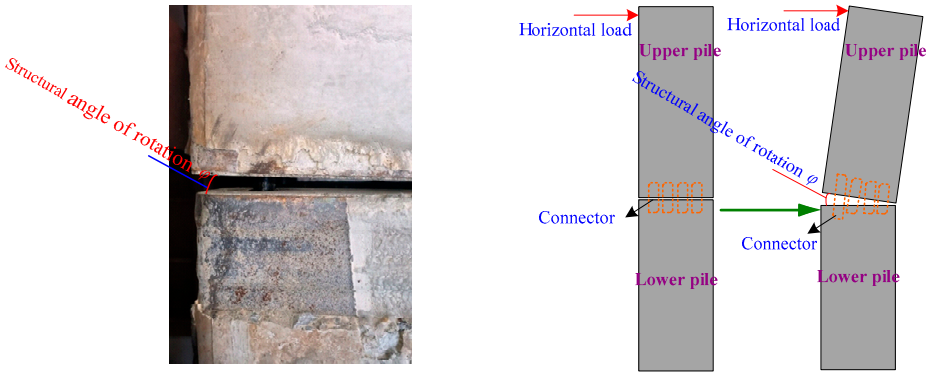


Figure 2. The angle of rotation diagram of mechanically connected pile structure. (**a**) Physical drawing. (**b**) Conceptual drawing.

(3) Synergistic force stage of upper and lower piles

The horizontal load continues to be applied, and when the structural angle of rotation exceeds this limit value, this plastic hinge begins to transmit bending moment and shear force, and the lower piles begin to participate in the force work. The displacement curve equations of the upper and lower piles are established separately and brought into the respective boundary conditions, and the system solution of the overall pile response is obtained by coupling the geometrical and mechanical relationship equations of the members.

Under the joint action of the pile and the soil of the mechanically connected piles, with the increase of external forces Q^0 and M^0 at the top of the upper pile, the rotation angle of the connectors gradually increases until it reaches the limit angle of rotation φ_0. Prior to this time, it is assumed that the lower piles are not subject to the transfer of moments and shear forces from the upper piles, that no displacements are generated, and that the action of the pile-soil at the top meets the assumption of the Winkel's elastic foundation beams as shown in Figure 3. In Figure 3, "0" denotes Section 0; "1" denotes Section 1; "2" denotes Section 2; "3" denotes Section 3.

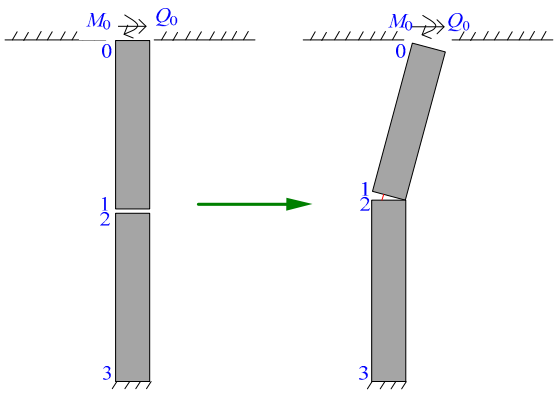


Figure 3. Deformation form of embedded pile body.

2.2. Dual-Pile Cooperative Work

When φ_1 reaches the limit value of the gap φ_0, which is determined by the construction of the joint, the angle of rotation reaches the limit state value. If the external load continues to be applied, the connection begins to transmit internal forces, and the lower pile begins to

displace horizontally. Then, the combination of load effects at the limit state is expressed as Equation (1). It is a guideline for determining at what stage the pile is stressed.

$$\overline{\varphi_1} = \overline{\varphi^0} = \delta_{\overline{\varphi_1}\overline{M_0}} \cdot \overline{M_0} + \delta_{\overline{\varphi_1}\overline{Q_0}} \cdot \overline{Q_0} \tag{1}$$

After the external load reaches the ultimate load and the load continues to be applied, the lower pile will be horizontally displaced under the driving of the connection; the upper and lower piles are driven by the connection, constituting a stressed whole. The deflection equations were established for the upper and lower piles, respectively. According to the force transmission characteristics of the mechanical connections, the deflection equations of the upper and lower piles are related to obtain the overall force state. The deflection equation of the upper pile is established based on the m-method. The second stage is basically the same as the first stage of the force condition, only the setting of boundary conditions is different; the deflection differential equation of the upper pile is

$$E_1 I_1 \frac{d^4 y}{dz^4} + m b_0 z y = 0,\ 0 < z < L_1 \tag{2}$$

In Equation (2), the calculated formulas for b_0 can be obtained from the specifications for the design of the foundation of highway bridges and culverts [19].

Let $\alpha_1 = \sqrt[5]{\frac{m b_0}{E_1 I_1}}$, then Equation (2) can be rewritten as

$$\frac{d^4 y}{dz^4} + {\alpha_1}^5 z y = 0 \tag{3}$$

Equation (3) can be solved by the power series method and dimensionless simplification:

$$\begin{cases} \overline{y(z)} = \overline{y_0} A_1 + \overline{\varphi_0} B_1 + \overline{M_0} C_1 + \overline{Q_0} D_1 \\ \overline{\varphi(z)} = \overline{y_0} A_2 + \overline{\varphi_0} B_2 + \overline{M_0} C_2 + \overline{Q_0} D_2 \\ \overline{M(z)} = \overline{y_0} A_3 + \overline{\varphi_0} B_3 + \overline{M_0} C_3 + \overline{Q_0} D_3 \\ \overline{Q(z)} = \overline{y_0} A_4 + \overline{\varphi_0} B_4 + \overline{M_0} C_4 + \overline{Q_0} D_4 \end{cases} \tag{4}$$

When the external loads on the upper pile are M^0 and Q^0, the horizontal displacement at its lower end is no longer 0 in the second stage of deformation, so the intermediate variables are introduced as the horizontal displacement and the angle of rotation angle in Section 1. Then, the boundary condition of the upper pile can be established as

$$\begin{cases} y(z = L_1) = y_1 \\ \varphi(z = L_1) = \varphi_1 \end{cases} \tag{5}$$

Bringing Equation (5) into Equations (1) and (2), it can obtain

$$\begin{cases} \overline{y_0} A_{11} + \overline{\varphi_0} B_{11} + \overline{M_0} C_{11} + \overline{Q_0} D_{11} = \overline{y_1} \\ \overline{y_0} A_{21} + \overline{\varphi_0} B_{21} + \overline{M_0} C_{21} + \overline{Q_0} D_{21} = \overline{\varphi_1} \end{cases} \tag{6}$$

Then, the solution is

$$\begin{cases} \overline{y_0} = \delta_{\overline{y_0}\,\overline{y_1}} \overline{y_1} + \delta_{\overline{y_0}\,\overline{\varphi_1}} \overline{\varphi_1} + \delta_{\overline{y_0}\overline{M_0}} \overline{M_0} + \delta_{\overline{y_0}\overline{Q_0}} \overline{Q_0} \\ \overline{\varphi_0} = \delta_{\overline{\varphi_0}\,\overline{y_1}} \overline{y_1} + \delta_{\overline{\varphi_0}\,\overline{\varphi_1}} \overline{\varphi_1} + \delta_{\overline{\varphi_0}\overline{M_0}} \overline{M_0} + \delta_{\overline{\varphi_0}\overline{Q_0}} \overline{Q_0} \end{cases} \tag{7}$$

where

$$\begin{cases} \delta_{\overline{y_0}\overline{y_1}} = -\frac{B_{21}}{A_{21}B_{11}-A_{11}B_{21}} \\ \delta_{\overline{y_0}\overline{\varphi_1}} = \frac{B_{11}}{A_{21}B_{11}-A_{11}B_{21}} \\ \delta_{\overline{y_0}\overline{M_0}} = \frac{B_{21}C_{11}-B_{11}C_{21}}{A_{21}B_{11}-A_{11}B_{21}} \\ \delta_{\overline{y_0}\overline{Q_0}} = \frac{B_{21}D_{11}-B_{11}D_{21}}{A_{21}B_{11}-A_{11}B_{21}} \\ \delta_{\overline{\varphi_0}\overline{y_1}} = \frac{A_{21}}{A_{21}B_{11}-A_{11}B_{21}} \\ \delta_{\overline{\varphi_0}\overline{\varphi_1}} = \frac{A_{11}}{A_{21}B_{11}-A_{11}B_{21}} \\ \delta_{\overline{\varphi_0}\overline{M_0}} = -\frac{A_{21}C_{11}-A_{11}C_{21}}{A_{21}B_{11}-A_{11}B_{21}} \\ \delta_{\overline{\varphi_0}\overline{Q_0}} = -\frac{A_{21}D_{11}-A_{11}D_{21}}{A_{21}B_{11}-A_{11}B_{21}} \end{cases} \quad (8)$$

These eight coefficients in Equation (8) are determined from the converted depth $\alpha_1 L_1$ in Section 1 and are given in Table 1.

Table 1. Coefficient of influence of upper pile boundary on pile top displacement response.

$\alpha_1 L_1$	$\delta_{\overline{y_0}\overline{y_1}}$	$\delta_{\overline{y_0}\overline{\varphi_1}}$	$\delta_{\overline{y_0}\overline{M_0}}$	$\delta_{\overline{y_0}\overline{Q_0}}$	$\delta_{\overline{\varphi_0}\overline{y_1}}$	$\delta_{\overline{\varphi_0}\overline{\varphi_1}}$	$\delta_{\overline{\varphi_0}\overline{M_0}}$	$\delta_{\overline{\varphi_0}\overline{Q_0}}$
0.0	1.00000	0.00000	0.00000	0.00000	0.00000	1.00000	0.00000	0.00000
0.1	1.00000	−0.10000	0.00500	0.00033	0.00000	1.00000	−0.10000	−0.00500
0.2	0.99999	−0.20000	0.02000	0.00267	0.00007	0.99999	−0.20000	−0.02000
0.3	0.99992	−0.29999	0.04500	0.00900	0.00034	0.99994	−0.30000	−0.04500
0.4	0.99966	−0.39992	0.07999	0.02133	0.00107	0.99974	−0.39996	−0.07999
0.5	0.99896	−0.49970	0.12495	0.04165	0.00260	0.99922	−0.49988	−0.12495
0.6	0.99741	−0.59910	0.17983	0.07192	0.00539	0.99806	−0.59962	−0.17983
0.7	0.99442	−0.69772	0.24448	0.11406	0.00997	0.99581	−0.69902	−0.24448
0.8	0.98913	−0.79492	0.31867	0.16985	0.01698	0.99185	−0.79783	−0.31867
0.9	0.98051	−0.88976	0.40199	0.24092	0.02706	0.98538	−0.89562	−0.40199
1.0	0.96718	−0.98085	0.49373	0.32854	0.04099	0.97539	−0.99179	−0.49375
1.1	0.94771	−1.06643	0.59294	0.43351	0.05937	0.96077	−1.08560	−0.59294
1.2	0.92031	−1.14417	0.69811	0.55589	0.08288	0.94021	−1.17605	−0.69811
1.3	0.88336	−1.21143	0.80737	0.69488	0.11189	0.91246	−1.26199	−0.80737
1.4	0.83530	−1.26524	0.91831	0.84855	0.14654	0.87636	−1.34213	−0.91831
1.5	0.77503	−1.30263	1.02816	1.01382	0.18656	0.83106	−1.41518	−1.02815
1.6	0.70202	−1.32086	1.13380	1.18632	0.23122	0.77612	−1.47990	−1.13379
1.7	0.61669	−1.31797	1.23219	1.36088	0.27927	0.71183	−1.53540	−1.23218
1.8	0.52033	−1.29295	1.32058	1.53179	0.32906	0.63909	−1.58115	−1.32059
1.9	0.41522	−1.24616	1.39688	1.69343	0.37861	0.55957	−1.61718	−1.39688
2.0	0.30444	−1.17928	1.45979	1.84091	0.42581	0.47549	−1.64405	−1.45979
2.2	0.07998	−0.99776	1.54549	2.08041	0.50555	0.30397	−1.67490	−1.54548
2.4	−0.12589	−0.77951	1.58566	2.23974	0.55677	0.14426	−1.68520	−1.58567
2.6	−0.29362	−0.55639	1.59617	2.32965	0.57544	0.01051	−1.68665	−1.59619
2.8	−0.41438	−0.35193	1.59262	2.37119	0.56380	−0.09103	−1.68717	−1.59265
3.0	−0.48805	−0.17917	1.58606	2.38548	0.52764	−0.16039	−1.69051	−1.58609
3.5	−0.50409	0.09557	1.58435	2.38891	0.37428	−0.22003	−1.71100	−1.58437
4.0	−0.37581	0.18363	1.59979	2.40075	0.20194	−0.18093	−1.73218	−1.59983

The expression for the displacement at the pile top for a pile with a fully consolidated bottom is

$$\overline{y_0} = \delta_{\overline{y_0}\overline{M_0}}\overline{M_0} + \delta_{\overline{y_0}\overline{Q_0}}\overline{Q_0} \quad (9)$$

$$\overline{y_0} = \delta_{\overline{y_0}\overline{M_0}}\overline{M_0} + \delta_{\overline{y_0}\overline{Q_0}}\overline{Q_0} + \delta_{\overline{y_0}\ \overline{\varphi_1}}\overline{\varphi_1} + \delta_{\overline{y_0}\ \overline{y_1}}\overline{y_1} \quad (10)$$

where $\delta_{\overline{y_0}\ \overline{y_1}}$ is negative, the horizontal displacement $\overline{y_1}$ at the pile bottom acts against the displacement $\overline{y_0}$ at the pile top (in the same direction).

Compared Equation (9) with Equation (10), it can be found that the larger the displacement at the bottom of the pile, the smaller the displacement at the pile top. When the pile bottom is not fully restrained, the external load is transferred from the pile body to the pile bottom to produce a positive horizontal displacement, and the horizontal displacement of

the pile bottom causes the soil body to produce part of the soil resistance to help balance the external load, which results in a decrease in the displacement of the pile body. During the loading of the mechanically connected piles, the pile top displacement will briefly stagnate at the beginning of the second stage, and the overall internal forces in the piles will be similarly redistributed. However, in general, the displacement generated at the bottom of the pile is not in the same direction as that at the top of the pile; in the case of consolidation and articulation, the displacement at the bottom of the pile is in the direction of 0, while in the case of the free boundary, the displacement at the bottom of the pile is in the opposite direction to that at the top of the pile. In this study, the positive direction displacement of the pile bottom is actually the displacement of the whole pile at the connection, and it is very reasonable to divide the pile body as a whole and consider the positive displacement here as the displacement at the bottom of the pile, and then explain it with the theory and further speculate the change of the pile body internal force in the next step. The displacement at the top of the pile can be further reduced if a boundary condition is added at the bottom of the pile to produce a positive displacement at the bottom of the pile. Rigid and flexible piles are temporarily unable to generate positive horizontal displacements under any embedment conditions.

Bringing Equation (7) into Equation (4), the internal forces in the upper pile can be expressed by the unknown $\overline{\varphi_1}$ and $\overline{y_1}$:

$$\begin{cases} \overline{y(z)} = \delta_{\overline{yy_1}}\overline{y_1} + \delta_{\overline{y\varphi_1}}\overline{\varphi_1} + \delta_{\overline{yM_0}}\overline{M_0} + \delta_{\overline{yQ_0}}\overline{Q_0} \\ \overline{\varphi(z)} = \delta_{\overline{\varphi y_1}}\overline{y_1} + \delta_{\overline{\varphi\varphi_1}}\overline{\varphi_1} + \delta_{\overline{\varphi M_0}}\overline{M_0} + \delta_{\overline{\varphi Q_0}}\overline{Q_0} \\ \overline{M(z)} = \delta_{\overline{My_1}}\overline{y_1} + \delta_{\overline{M\varphi_1}}\overline{\varphi_1} + \delta_{\overline{MM_0}}\overline{M_0} + \delta_{\overline{MQ_0}}\overline{Q_0} \\ \overline{Q(z)} = \delta_{\overline{Qy_1}}\overline{y_1} + \delta_{\overline{Q\varphi_1}}\overline{\varphi_1} + \delta_{\overline{QM_0}}\overline{M_0} + \delta_{\overline{QQ_0}}\overline{Q_0} \end{cases}, \ 0 \le L \le L_1 \tag{11}$$

where

$$\begin{cases} \delta_{\overline{yy_1}} = \frac{B_1A_{21}-A_1B_{21}}{A_{21}B_{11}-A_{11}B_{21}} \\ \delta_{\overline{y\varphi_1}} = \frac{A_1B_{11}-B_1A_{11}}{A_{21}B_{11}-A_{11}B_{21}} \\ \delta_{\overline{yM_0}} = \frac{A_1(B_{21}C_{11}-B_{11}C_{21})-B_1(A_{21}C_{11}-A_{11}C_{21})}{A_{21}B_{11}-A_{11}B_{21}} + C_1 \\ \delta_{\overline{yQ_0}} = \frac{A_1(B_{21}C_{11}-B_{11}C_{21})-B_1(A_{21}C_{11}-A_{11}C_{21})}{A_{21}B_{11}-A_{11}B_{21}} + D_1 \\ \delta_{\overline{\varphi y_1}} = \frac{B_2A_{21}-A_2B_{21}}{A_{21}B_{11}-A_{11}B_{21}} \\ \delta_{\overline{\varphi\varphi_1}} = \frac{A_2B_{11}-B_2A_{11}}{A_{21}B_{11}-A_{11}B_{21}} \\ \delta_{\overline{\varphi M_0}} = \frac{A_1(B_{21}C_{11}-B_{11}C_{21})-B_1(A_{21}C_{11}-A_{11}C_{21})}{A_{21}B_{11}-A_{11}B_{21}} + C_2 \\ \delta_{\overline{\varphi Q_0}} = \frac{A_1(B_{21}C_{11}-B_{11}C_{21})-B_1(A_{21}C_{11}-A_{11}C_{21})}{A_{21}B_{11}-A_{11}B_{21}} + D_2 \\ \delta_{\overline{My_1}} = \frac{B_3A_{21}-A_2B_{21}}{A_{21}B_{11}-A_{11}B_{21}} \\ \delta_{\overline{M\varphi_1}} = \frac{A_3B_{11}-B_2A_{11}}{A_{21}B_{11}-A_{11}B_{21}} \\ \delta_{\overline{MM_0}} = \frac{A_1(B_{21}C_{11}-B_{11}C_{21})-B_1(A_{21}C_{11}-A_{11}C_{21})}{A_{21}B_{11}-A_{11}B_{21}} + C_3 \\ \delta_{\overline{MQ_0}} = \frac{A_1(B_{21}C_{11}-B_{11}C_{21})-B_1(A_{21}C_{11}-A_{11}C_{21})}{A_{21}B_{11}-A_{11}B_{21}} + D_3 \\ \delta_{\overline{Qy_1}} = \frac{B_4A_{21}-A_2B_{21}}{A_{21}B_{11}-A_{11}B_{21}} \\ \delta_{\overline{Q\varphi_1}} = \frac{A_4B_{11}-B_2A_{11}}{A_{21}B_{11}-A_{11}B_{21}} \\ \delta_{\overline{QM_0}} = \frac{A_1(B_{21}C_{11}-B_{11}C_{21})-B_1(A_{21}C_{11}-A_{11}C_{21})}{A_{21}B_{11}-A_{11}B_{21}} + C_4 \\ \delta_{\overline{QQ_0}} = \frac{A_1(B_{21}C_{11}-B_{11}C_{21})-B_1(A_{21}C_{11}-A_{11}C_{21})}{A_{21}B_{11}-A_{11}B_{21}} + D_4 \end{cases} \tag{12}$$

The 16 coefficients $\delta_{\overline{y}\ \overline{y_1}}$–$\delta_{\overline{QQ_0}}$ in Equation (12) represent the effects of the four boundary conditions $\overline{y_1}$, $\overline{\varphi_1}$, $\overline{M_0}$, and $\overline{Q_0}$ on the internal forces $\overline{y}$, $\overline{\varphi}$, $\overline{M}$, and $\overline{Q}$ in any cross-section, and the combination of their effects is the value of the internal force in that cross-section, which is used for calculating the response of the pile body in the upper pile. When L = 0, the values of $A_1 - D_4$ at $\alpha_1 L = 0$ reveals that the expression is exactly the same as that of $\delta_{\overline{y_0y_1}} - \delta_{\overline{QQ_0}}$ in Equation (8), thus enabling the validation of the correctness of Equation (12).

When L = L1, the internal force in Section 1 at the bottom of the upper pile can be obtained as Equation (13).

$$\begin{cases} \overline{M}(z=L_1) = \delta_{\overline{M_1}\overline{y_1}}\overline{y_1} + \delta_{\overline{M_1}\overline{\varphi_1}}\overline{\varphi_1} + \delta_{\overline{M_1}\overline{M_0}}\overline{M_0} + \delta_{\overline{M_1}\overline{Q_0}}\overline{Q_0} \\ \overline{Q}(z=L_1) = \delta_{\overline{Q_1}\overline{y_1}}\overline{y_1} + \delta_{\overline{Q_1}\overline{\varphi_1}}\overline{\varphi_1} + \delta_{\overline{Q_1}\overline{M_0}}\overline{M_0} + \delta_{\overline{Q_1}\overline{Q_0}}\overline{Q_0} \end{cases} \tag{13}$$

where

$$\begin{cases} \delta_{\overline{M_1}\overline{y_1}} = \frac{B_{31}A_{21}-A_{31}B_{21}}{A_{21}B_{11}-A_{11}B_{21}} \\ \delta_{\overline{M_1}\overline{\varphi_1}} = \frac{A_{31}B_{11}-B_{31}A_{11}}{A_{21}B_{11}-A_{11}B_{21}} \\ \delta_{\overline{M_1}\overline{M_0}} = \frac{A_{31}(B_{21}C_{11}-B_{11}C_{21})-B_{31}(A_{21}C_{11}-A_{11}C_{21})}{A_{21}B_{11}-A_{11}B_{21}} + C_{31} \\ \delta_{\overline{M_1}\overline{Q_0}} = \frac{A_{31}(B_{21}D_{11}-B_{11}D_{21})-B_{31}(A_{21}D_{11}-A_{11}D_{21})}{A_{21}B_{11}-A_{11}B_{21}} + D_{31} \\ \delta_{\overline{Q_1}\overline{y_1}} = \frac{B_{41}A_{21}-A_{41}B_{21}}{A_{21}B_{11}-A_{11}B_{21}} \\ \delta_{\overline{Q_1}\overline{\varphi_1}} = \frac{A_{41}B_{11}-B_{41}A_{11}}{A_{21}B_{11}-A_{11}B_{21}} \\ \delta_{\overline{Q_1}\overline{M_0}} = \frac{A_{41}(B_{21}C_{11}-B_{11}C_{21})-B_{41}(A_{21}C_{11}-A_{11}C_{21})}{A_{21}B_{11}-A_{11}B_{21}} + C_{41} \\ \delta_{\overline{Q_1}\overline{Q_0}} = \frac{A_{41}(B_{21}D_{11}-B_{11}D_{21})-B_{41}(A_{21}D_{11}-A_{11}D_{21})}{A_{21}B_{11}-A_{11}B_{21}} + D_{41} \end{cases} \tag{14}$$

These eight coefficients in Equation (14) are determined solely from the converted depth $\alpha_1 L_1$ in Section 1 and are given in Table 2.

Table 2. Coefficients of influence of the upper pile boundary on the internal force response in Section 1.

$\alpha_1 L_1$	$\delta_{\overline{M_1}\overline{y_1}}$	$\delta_{\overline{M_1}\overline{\varphi_1}}$	$\delta_{\overline{M_1}\overline{M_0}}$	$\delta_{\overline{M_1}\overline{Q_0}}$	$\delta_{\overline{Q_1}\overline{y_1}}$	$\delta_{\overline{Q_1}\overline{\varphi_1}}$	$\delta_{\overline{Q_1}\overline{M_0}}$	$\delta_{\overline{Q_1}\overline{Q_0}}$
0.0	0.00000	0.00000	1.00000	0.00000	0.00000	0.00000	0.00000	1.00000
0.1	−0.00017	0.00001	1.00000	0.10000	−0.00500	0.00017	0.00000	1.00000
0.2	−0.00133	0.00014	0.99999	0.20000	−0.02000	0.00133	−0.00007	0.99999
0.3	−0.00450	0.00068	0.99994	0.29999	−0.04500	0.00450	−0.00034	0.99992
0.4	−0.01067	0.00214	0.99974	0.39992	−0.08000	0.01067	−0.00107	0.99966
0.5	−0.02082	0.00520	0.99922	0.49969	−0.12497	0.02082	−0.00260	0.99896
0.6	−0.03597	0.01079	0.99806	0.59909	−0.17989	0.03597	−0.00540	0.99741
0.7	−0.05704	0.01996	0.99581	0.69772	−0.24467	0.05702	−0.00996	0.99442
0.8	−0.08497	0.03398	0.99184	0.79492	−0.31917	0.08497	−0.01699	0.98914
0.9	−0.12055	0.05419	0.98538	0.88977	−0.40312	0.12056	−0.02706	0.98050
1.0	−0.16447	0.08209	0.97540	0.98087	−0.49609	0.16447	−0.04096	0.96720
1.1	−0.21717	0.11910	0.96076	1.06642	−0.59746	0.21717	−0.05937	0.94770
1.2	−0.27877	0.16652	0.94020	1.14417	−0.70631	0.27877	−0.08288	0.92032
1.3	−0.34898	0.22532	0.91246	1.21143	−0.82146	0.34897	−0.11188	0.88337
1.4	−0.42698	0.29602	0.87634	1.26524	−0.94111	0.42873	−0.14923	0.83349
1.5	−0.51144	0.37841	0.83103	1.30260	−1.06438	0.51146	−0.18659	0.77501
1.6	−0.60044	0.47147	0.77611	1.32084	−1.18843	0.60044	−0.23125	0.70203
1.7	−0.69168	0.57337	0.71181	1.31794	−1.31162	0.69173	−0.27937	0.61661
1.8	−0.78259	0.68141	0.63906	1.29292	−1.43221	0.78260	−0.32910	0.52030
1.9	−0.87067	0.79242	0.55953	1.24615	−1.54875	0.87067	−0.37866	0.41524
2.0	−0.95371	0.90297	0.47545	1.17925	−1.66040	0.95371	−0.42584	0.30446
2.2	−1.09885	1.11028	0.30389	0.99772	−1.86835	1.09885	−0.50559	0.08003
2.4	−1.21330	1.28484	0.14416	0.77944	−2.05964	1.21332	−0.55690	−0.12590
2.6	−1.30183	1.42061	0.01039	0.55624	−2.24232	1.30187	−0.57544	−0.29352
2.8	−1.37369	1.52161	−0.09126	0.35182	−2.42376	1.37374	−0.56387	−0.41420
3.0	−1.43774	1.59667	−0.16074	0.17894	−2.60815	1.43780	−0.52806	−0.48816
3.5	−1.59636	1.72536	−0.22055	−0.09593	−3.08241	1.59642	−0.37477	−0.50400
4.0	−1.76223	1.82594	−0.18144	−0.18388	−3.54605	1.76217	−0.20311	−0.37654

Note: The two unknown variables $\overline{y_1}$ and $\overline{\varphi_1}$ in Equation (13) will be eliminated by the internal force case of the lower pile.

2.3. Solving for Internal Forces in the Lower Pile

The force form of the lower pile in the stage of double-pile cooperative work is shown in Figure 4. It is first assumed that the lower pile is through the length and its top is flush with the ground. The lower deflection curve of the through-length pile is ensured to be the same as the actual deflection curve by ensuring that the deflection of the through-length pile in Section 1 is equal to the actual deflection. For a virtual through-length pile with length $(L_1 + L_2)$ and flexural stiffness E_2I_2, the soil resistance on the pile side satisfies Winkle's elastic foundation model; the basic deflection equation is expressed as Equation (15).

$$E_2I_2\frac{d^4y}{dz^4} + mb_0zy = 0,\ (0 \le z \le L_1 + L_2) \tag{15}$$

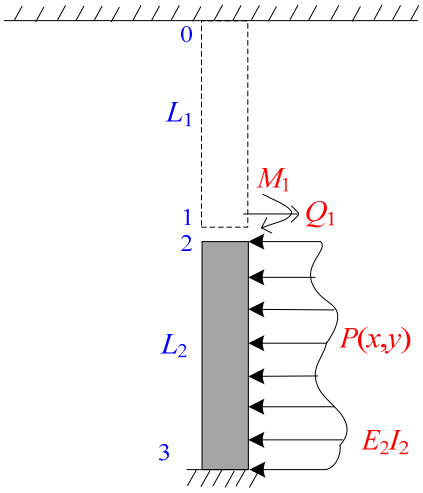


Figure 4. The force form of the lower pile in the stage of double-pile cooperative work.

Let $\alpha_2 = \sqrt[5]{\frac{mb_0}{E_2I_2}}$, then it can obtain

$$\frac{d^4y}{dz^4} + {\alpha_2}^5zy = 0 \tag{16}$$

The solution of the through-length pile deflection equation is obtained by solving the power series method and simplifying it by dimensionless simplification:

$$\begin{cases} \overline{y(z)}^{\Delta} = \overline{y_0}^{\Delta}A_1 + \overline{\varphi_0}^{\Delta}B_1 + \overline{M_0}^{\Delta}C_1 + \overline{Q_0}^{\Delta}D_1 \\ \overline{\varphi(z)}^{\Delta} = \overline{y_0}^{\Delta}A_2 + \overline{\varphi_0}^{\Delta}B_2 + \overline{M_0}^{\Delta}C_2 + \overline{Q_0}^{\Delta}D_2 \\ \overline{M(z)}^{\Delta} = \overline{y_0}^{\Delta}A_3 + \overline{\varphi_0}^{\Delta}B_3 + \overline{M_0}^{\Delta}C_3 + \overline{Q_0}^{\Delta}D_3 \\ \overline{Q(z)}^{\Delta} = \overline{y_0}^{\Delta}A_4 + \overline{\varphi_0}^{\Delta}B_4 + \overline{M_0}^{\Delta}C_4 + \overline{Q_0}^{\Delta}D_4 \end{cases} \tag{17}$$

where $\overline{y_0}^{\Delta}$, $\overline{\varphi_0}^{\Delta}$, $\overline{M_0}^{\Delta}$, and $\overline{Q_0}^{\Delta}$ denote the pile top displacement, angle of rotation, external force and external moment of the virtual through-length pile, respectively. Since the through-length piles are fictional equivalents, $\overline{y_0}^{\Delta}$, $\overline{\varphi_0}^{\Delta}$, $\overline{M_0}^{\Delta}$, and $\overline{Q_0}^{\Delta}$ do not actually exist and are also equivalents, they are distinguished by the angle of rotation notation Δ.

When $L_1 \le L \le L_1 + L_2$, the displacements and internal forces of the through-length pile are exactly the same as the actual situation, i.e.,:

$$\begin{cases} \overline{y(z)} = \delta_{\overline{y}^{\Delta}\overline{y_2}^{\Delta}} \cdot \overline{y}_2 + \delta_{\overline{y}^{\Delta}\overline{\varphi_2}^{\Delta}} \cdot \overline{\varphi}_2 \\ \overline{\varphi(z)} = \delta_{\overline{\varphi}^{\Delta}\overline{y_2}^{\Delta}} \cdot \overline{y}_2 + \delta_{\overline{\varphi}^{\Delta}\overline{\varphi_2}^{\Delta}} \cdot \overline{\varphi}_2 \\ \overline{M(z)} = \delta_{\overline{M}^{\Delta}\overline{y_2}^{\Delta}} \cdot \overline{y}_2 + \delta_{\overline{M}^{\Delta}\overline{\varphi_2}^{\Delta}} \cdot \overline{\varphi}_2 \\ \overline{Q(z)} = \delta_{\overline{Q}^{\Delta}\overline{y_2}^{\Delta}} \cdot \overline{y}_2 + \delta_{\overline{Q}^{\Delta}\overline{\varphi_2}^{\Delta}} \cdot \overline{\varphi}_2 \end{cases}, \; L_1 \le L \le L_1 + L_2 \tag{18}$$

The solutions of the deflection equation for a connected pile with external loads M_0 and Q_0, upper bending stiffness E_1I_1 and lower bending stiffness E_2I_2 in the stage of double-pile cooperative work are

$$\begin{cases} \overline{y(z)} = \delta_{\overline{y}\overline{y_1}}\overline{y_1} + \delta_{\overline{y}\overline{\varphi_1}}\overline{\varphi_1} + \delta_{\overline{y}\overline{M_0}}\overline{M_0} + \delta_{\overline{y}\overline{Q_0}}\overline{Q_0} \\ \overline{\varphi(z)} = \delta_{\overline{\varphi}\overline{y_1}}\overline{y_1} + \delta_{\overline{\varphi}\overline{\varphi_1}}\overline{\varphi_1} + \delta_{\overline{\varphi}\overline{M_0}}\overline{M_0} + \delta_{\overline{\varphi}\overline{Q_0}}\overline{Q_0} \\ \overline{M(z)} = \delta_{\overline{M}\overline{y_1}}\overline{y_1} + \delta_{\overline{M}\overline{\varphi_1}}\overline{\varphi_1} + \delta_{\overline{M}\overline{M_0}}\overline{M_0} + \delta_{\overline{M}\overline{Q_0}}\overline{Q_0} \\ \overline{Q(z)} = \delta_{\overline{Q}\overline{y_1}}\overline{y_1} + \delta_{\overline{Q}\overline{\varphi_1}}\overline{\varphi_1} + \delta_{\overline{Q}\overline{M_0}}\overline{M_0} + \delta_{\overline{Q}\overline{Q_0}}\overline{Q_0} \end{cases}, \; 0 \le L \le L_1 \tag{19}$$

and

$$\begin{cases} \overline{y(z)} = \delta_{\overline{y}^{\Delta}\overline{y_2}^{\Delta}} \cdot \overline{y_2} + \delta_{\overline{y}^{\Delta}\overline{\varphi_2}^{\Delta}} \cdot \overline{\varphi_2} \\ \overline{\varphi(z)} = \delta_{\overline{\varphi}^{\Delta}\overline{y_2}^{\Delta}} \cdot \overline{y_2} + \delta_{\overline{\varphi}^{\Delta}\overline{\varphi_2}^{\Delta}} \cdot \overline{\varphi_2} \\ \overline{M(z)} = \delta_{\overline{M}^{\Delta}\overline{y_2}^{\Delta}} \cdot \overline{y_2} + \delta_{\overline{M}^{\Delta}\overline{\varphi_2}^{\Delta}} \cdot \overline{\varphi_2} \\ \overline{Q(z)} = \delta_{\overline{Q}^{\Delta}\overline{y_2}^{\Delta}} \cdot \overline{y_2} + \delta_{\overline{Q}^{\Delta}\overline{\varphi_2}^{\Delta}} \cdot \overline{\varphi_2} \end{cases} L_1 \le L \le L_1 + L_2 \tag{20}$$

where $\overline{y_1}$, $\overline{\varphi_1}$, $\overline{y_2}$ and $\overline{\varphi_2}$ are unknown intermediate variables.

Assuming that the connectors do not deform during normal operation, it can be ensured that Sections 2 and 3 maintain the same horizontal displacement, and the difference in the angle of rotation is the structural angle of rotation φ^0. Then, the geometric conditions can be summarised as

$$\begin{cases} \overline{y_1} = \overline{y_2} \\ \overline{\varphi_1} + \overline{\varphi^0} = \overline{\varphi_2} \end{cases} \tag{21}$$

The connection is working with 100 percent transfer of internal forces to the upper and lower piles, so there is no weakening of internal forces in Sections 2 and 3, then the equilibrium conditions can be summarised as

$$\begin{cases} \overline{M_1} = \overline{M_2} \\ \overline{Q_1} = \overline{Q_2} \end{cases} \tag{22}$$

2.4. Solution for Internal Force Equations

Bringing Equations (21) and (22) into Equations (11) and (18) yields a system of equations:

$$\begin{cases} \delta_{\overline{M_1}\overline{y_1}}\overline{y_1} + \delta_{\overline{M_1}\cdot\overline{\varphi_1}}\overline{\varphi_1} + \delta_{\overline{M_1}\cdot\overline{M_0}}\overline{M_0} + \delta_{\overline{M_1}\cdot\overline{Q_0}}\overline{Q_0} = \delta_{\overline{M_2}^{\Delta}\overline{y_2}^{\Delta}} \cdot \overline{y_1} + \delta_{\overline{M_2}^{\Delta}\overline{\varphi_2}^{\Delta}} \cdot \left(\overline{\varphi_1} + \overline{\varphi^0}\right) \\ \delta_{\overline{Q_1}\cdot\overline{y_1}}\overline{y_1} + \delta_{\overline{Q_1}\cdot\overline{\varphi_1}}\overline{\varphi_1} + \delta_{\overline{Q_1}\cdot\overline{M_0}}\overline{M_0} + \delta_{\overline{Q_1}\overline{Q_0}}\overline{Q_0} = \delta_{\overline{Q_2}^{\Delta}\overline{y_2}^{\Delta}} \cdot \overline{y_1} + \delta_{\overline{Q_2}^{\Delta}\overline{\varphi_2}^{\Delta}} \cdot \left(\overline{\varphi_1} + \overline{\varphi^0}\right) \end{cases} \tag{23}$$

The solution for Equation (23) is

$$\begin{cases} \overline{y_1} = \delta_{\overline{y_1}\overline{\varphi^0}} \cdot \overline{\varphi^0} + \delta_{\overline{y_1}\overline{M_0}} \cdot \overline{M_0} + \delta_{\overline{y_1}\overline{Q_0}} \cdot \overline{Q_0} \\ \overline{\varphi_1} = \delta_{\overline{\varphi_1}\overline{\varphi^0}} \cdot \overline{\varphi^0} + \delta_{\overline{\varphi_1}\overline{M_0}} \cdot \overline{M_0} + \delta_{\overline{\varphi_1}\overline{Q_0}} \cdot \overline{Q_0} \end{cases} \tag{24}$$

where

$$\begin{cases} \delta_{\overline{y_1}\overline{\varphi^0}} = \dfrac{\left(\delta_{\overline{Q_1}\overline{\varphi_1}}-\delta_{\overline{Q_2}^{\Delta}\overline{\varphi_2}^{\Delta}}\right)\delta_{\overline{M_2}^{\Delta}\overline{\varphi_2}^{\Delta}}-\left(\delta_{\overline{M_1}\overline{\varphi_1}}-\delta_{\overline{M_2}^{\Delta}\overline{\varphi_2}^{\Delta}}\right)\delta_{\overline{Q_2}^{\Delta}\overline{\varphi_2}^{\Delta}}}{\left(\delta_{\overline{M_1}\overline{y_1}}-\delta_{\overline{M_2}^{\Delta}\overline{y_2}^{\Delta}}\right)\left(\delta_{\overline{Q_1}\overline{\varphi_1}}-\delta_{\overline{Q_2}^{\Delta}\overline{\varphi_2}^{\Delta}}\right)-\left(\delta_{\overline{Q_1}\overline{y_1}}-\delta_{\overline{Q_2}^{\Delta}\overline{y_2}^{\Delta}}\right)\left(\delta_{\overline{M_1}\overline{\varphi_1}}-\delta_{\overline{M_2}^{\Delta}\overline{\varphi_2}^{\Delta}}\right)} \\ \delta_{\overline{y_1}\overline{M_0}} = \dfrac{-\left(\delta_{\overline{Q_1}\overline{\varphi_1}}-\delta_{\overline{Q_2}^{\Delta}\overline{\varphi_2}^{\Delta}}\right)\delta_{\overline{M_1}\overline{M_0}}+\left(\delta_{\overline{M_1}\overline{\varphi_1}}-\delta_{\overline{M_2}^{\Delta}\overline{\varphi_2}^{\Delta}}\right)\delta_{\overline{Q_1}\overline{M_0}}}{\left(\delta_{\overline{M_1}\overline{y_1}}-\delta_{\overline{M_2}^{\Delta}\overline{y_2}^{\Delta}}\right)\left(\delta_{\overline{Q_1}\overline{\varphi_1}}-\delta_{\overline{Q_2}^{\Delta}\overline{\varphi_2}^{\Delta}}\right)-\left(\delta_{\overline{Q_1}\overline{y_1}}-\delta_{\overline{Q_2}^{\Delta}\overline{y_2}^{\Delta}}\right)\left(\delta_{\overline{M_1}\overline{\varphi_1}}-\delta_{\overline{M_2}^{\Delta}\overline{\varphi_2}^{\Delta}}\right)} \\ \delta_{\overline{y_1}\overline{Q_0}} = \dfrac{-\left(\delta_{\overline{Q_1}\overline{\varphi_1}}-\delta_{\overline{Q_2}^{\Delta}\overline{\varphi_2}^{\Delta}}\right)\delta_{\overline{M_1}\overline{Q_0}}+\left(\delta_{\overline{M_1}\overline{\varphi_1}}-\delta_{\overline{M_2}^{\Delta}\overline{\varphi_2}^{\Delta}}\right)\delta_{\overline{Q_1}\overline{\varphi_0}}}{\left(\delta_{\overline{M_1}\overline{y_1}}-\delta_{\overline{M_2}^{\Delta}\overline{\varphi_1}^{\Delta}}\right)\left(\delta_{\overline{Q_1}\overline{\varphi_1}}-\delta_{\overline{Q_2}^{\Delta}\overline{\varphi_2}^{\Delta}}\right)-\left(\delta_{\overline{Q_1}\overline{y_1}}-\delta_{\overline{Q_2}^{\Delta}\overline{y_2}^{\Delta}}\right)\left(\delta_{\overline{M_1}\overline{\varphi_1}}-\delta_{\overline{M_2}^{\Delta}\overline{\varphi_2}^{\Delta}}\right)} \\ \delta_{\overline{\varphi_1}\overline{\varphi^0}} = \dfrac{-\left(\delta_{\overline{Q_1}\overline{y_1}}-\delta_{\overline{Q_2}^{\Delta}\overline{y_2}^{\Delta}}\right)\delta_{\overline{M_2}^{\Delta}\overline{\varphi_2}^{\Delta}}+\left(\delta_{\overline{M_1}\overline{y_1}}-\delta_{\overline{M_2}^{\Delta}\overline{y_2}^{\Delta}}\right)\delta_{\overline{Q_2}^{\Delta}\overline{\varphi_2}^{\Delta}}}{\left(\delta_{\overline{M_1}\overline{y_1}}-\delta_{\overline{M_2}^{\Delta}\overline{y_2}^{\Delta}}\right)\left(\delta_{\overline{Q_1}\overline{\varphi_1}}-\delta_{\overline{Q_2}^{\Delta}\overline{\varphi_2}^{\Delta}}\right)-\left(\delta_{\overline{Q_1}\overline{\varphi_1}}-\delta_{\overline{Q_2}^{\Delta}\overline{y_2}^{\Delta}}\right)\left(\delta_{\overline{M_1}\overline{\varphi_1}}-\delta_{\overline{M_2}^{\Delta}\overline{\varphi_2}^{\Delta}}\right)} \\ \delta_{\overline{\varphi_1}\overline{M_0}} = \dfrac{\left(\delta_{\overline{Q_1}\overline{y_1}}-\delta_{\overline{Q_2}^{\Delta}\overline{y_2}^{\Delta}}\right)\delta_{\overline{M_1}\overline{Q_0}}-\left(\delta_{\overline{M_1}\overline{y_1}}-\delta_{\overline{M_2}^{\Delta}\overline{y_2}^{\Delta}}\right)\delta_{\overline{Q_1}\overline{M_0}}}{\left(\delta_{\overline{M_1}\overline{y_1}}-\delta_{\overline{M_2}^{\Delta}\overline{y_2}^{\Delta}}\right)\left(\delta_{\overline{Q_1}\overline{\varphi_1}}-\delta_{\overline{Q_2}^{\Delta}\overline{\varphi_2}^{\Delta}}\right)-\left(\delta_{\overline{Q_1}\overline{y_1}}-\delta_{\overline{Q_2}^{\Delta}\overline{y_2}^{\Delta}}\right)\left(\delta_{\overline{M_1}\overline{\varphi_1}}-\delta_{\overline{M_2}^{\Delta}\overline{\varphi_2}^{\Delta}}\right)} \\ \delta_{\overline{\varphi_1}\overline{Q_0}} = \dfrac{\left(\delta_{\overline{Q_1}\overline{y_1}}-\delta_{\overline{Q_2}^{\Delta}\overline{y_2}^{\Delta}}\right)\delta_{\overline{M_1}\overline{Q_0}}-\left(\delta_{\overline{Q_1}\overline{y_1}}-\delta_{\overline{Q_2}^{\Delta}\overline{y_2}^{\Delta}}\right)\delta_{\overline{Q_1}\overline{Q_0}}}{\left(\delta_{\overline{M_1}\overline{y_1}}-\delta_{\overline{M_2}^{\Delta}\overline{y_2}^{\Delta}}\right)\left(\delta_{\overline{Q_1}\overline{\varphi_1}}-\delta_{\overline{Q_2}^{\Delta}\overline{\varphi_2}^{\Delta}}\right)-\left(\delta_{\overline{Q_1}\overline{y_1}}-\delta_{\overline{Q_2}^{\Delta}\overline{y_2}^{\Delta}}\right)\left(\delta_{\overline{M_1}\overline{\varphi_1}}-\delta_{\overline{M_2}^{\Delta}\overline{\varphi_2}^{\Delta}}\right)} \end{cases} \tag{25}$$

When the bending stiffness of the upper and lower piles is the same, $\alpha_1 = \alpha_2$. The internal force response coefficients for mechanically connected piles with fixed constraints at the pile bottom in Section 1 are listed in Table 3 and are controlled by $\alpha_1 L_1$. The internal force response coefficients for mechanically connected piles with fixed constraints in Section 2 are listed in Table 4 and are controlled by $\alpha_2 L_1$.

Table 3. Internal force response coefficients for mechanically connected piles with fixed constraints are in Section 1.

$\alpha_1 L_1$	$\delta_{\overline{M_1}\overline{y_1}}$	$\delta_{\overline{M_1}\overline{\varphi_1}}$	$\delta_{\overline{M_1}\overline{M_0}}$	$\delta_{\overline{Q_1}\overline{M_0}}$	$\delta_{\overline{Q_1}\overline{y_1}}$	$\delta_{\overline{Q_1}\overline{\varphi_1}}$	$\delta_{\overline{Q_1}\overline{M_0}}$	$\delta_{\overline{Q_1}\overline{Q_0}}$
0.0	0.00000	0.00000	1.00000	0.00000	0.00000	0.00000	0.00000	1.00000
0.1	−0.00017	0.00001	1.00000	0.10000	−0.00500	0.00017	0.00000	1.00000
0.2	−0.00133	0.00014	0.99999	0.20000	−0.02000	0.00133	−0.00007	0.99999
0.3	−0.00450	0.00068	0.99994	0.29999	−0.04500	0.00450	−0.00034	0.99992
0.4	−0.01067	0.00214	0.99974	0.39992	−0.08000	0.01067	−0.00107	0.99966
0.5	−0.02082	0.00520	0.99922	0.49969	−0.12497	0.02082	−0.00260	0.99896
0.6	−0.03597	0.01079	0.99806	0.59909	−0.17989	0.03597	−0.00540	0.99741
0.7	−0.05704	0.01996	0.99581	0.69772	−0.24467	0.05702	−0.00996	0.99442
0.8	−0.08497	0.03398	0.99184	0.79492	−0.31917	0.08497	−0.01699	0.98914
0.9	−0.12055	0.05419	0.98538	0.88977	−0.40312	0.12056	−0.02706	0.98050
1.0	−0.16447	0.08209	0.97540	0.98087	−0.49609	0.16447	−0.04096	0.96720
1.1	−0.21717	0.11910	0.96076	1.06642	−0.59746	0.21717	−0.05937	0.94770
1.2	−0.27877	0.16652	0.94020	1.14417	−0.70631	0.27877	−0.08288	0.92032
1.3	−0.34898	0.22532	0.91246	1.21143	−0.82146	0.34897	−0.11188	0.88337
1.4	−0.42698	0.29602	0.87634	1.26524	−0.94111	0.42873	−0.14923	0.83349
1.5	−0.51144	0.37841	0.83103	1.30260	−1.06438	0.51146	−0.18659	0.77501
1.6	−0.60044	0.47147	0.77611	1.32084	−1.18843	0.60044	−0.23125	0.70203
1.7	−0.69168	0.57337	0.71181	1.31794	−1.31162	0.69173	−0.27937	0.61661
1.8	−0.78259	0.68141	0.63906	1.29292	−1.43221	0.78260	−0.32910	0.52030
1.9	−0.87067	0.79242	0.55953	1.24615	−1.54875	0.87067	−0.37866	0.41524
2.0	−0.95371	0.90297	0.47545	1.17925	−1.66040	0.95371	−0.42584	0.30446
2.2	−1.09885	1.11028	0.30389	0.99772	−1.86835	1.09885	−0.50559	0.08003
2.4	−1.21330	1.28484	0.14416	0.77944	−2.05964	1.21332	−0.55690	−0.12590

Table 3. *Cont.*

$\alpha_1 L_1$	$\delta_{\overline{M_1}\overline{y_1}}$	$\delta_{\overline{M_1}\overline{\varphi_1}}$	$\delta_{\overline{M_1}M_0}$	$\delta_{\overline{Q_1}M_0}$	$\delta_{\overline{Q_1}\overline{y_1}}$	$\delta_{\overline{Q_1}\overline{\varphi_1}}$	$\delta_{\overline{Q_1}M_0}$	$\delta_{\overline{Q_1}Q_0}$
2.6	−1.30183	1.42061	0.01039	0.55624	−2.24232	1.30187	−0.57544	−0.29352
2.8	−1.37369	1.52161	−0.09126	0.35182	−2.42376	1.37374	−0.56387	−0.41420
3.0	−1.43774	1.59667	−0.16074	0.17894	−2.60815	1.43780	−0.52806	−0.48816
3.5	−1.59636	1.72536	−0.22055	−0.09593	−3.08241	1.59642	−0.37477	−0.50400
4.0	−1.76223	1.82594	−0.18144	−0.18388	−3.54605	1.76217	−0.20311	−0.37654

Table 4. Internal force response coefficients for mechanically connected piles with fixed constraints are in Section 2.

$\alpha_2 L_1$	$\delta_{\overline{y_2}^{\Delta}\overline{y_2}^{\Delta}}$	$\delta_{\overline{y_2}^{\Delta}\overline{\varphi_2}^{\Delta}}$	$\delta_{\overline{\varphi_2}^{\Delta}\overline{y_2}^{\Delta}}$	$\delta_{\overline{\varphi_2}^{\Delta}\overline{\varphi_2}^{\Delta}}$	$\delta_{\overline{M_2}^{\Delta}\overline{y_2}^{\Delta}}$	$\delta_{\overline{M_2}^{\Delta}\overline{\varphi_2}^{\Delta}}$	$\delta_{\overline{Q_2}^{\Delta}\overline{y_2}^{\Delta}}$	$\delta_{\overline{Q_2}^{\Delta}\overline{\varphi_2}^{\Delta}}$
0.00	1.00000	0.00000	0.00000	1.00000	−1.00043	−1.50127	1.08320	1.00040
0.10	1.00000	0.00000	0.00000	1.00000	−1.04172	−1.52620	1.18248	1.04169
0.20	1.00000	0.00000	0.00000	1.00000	−1.08195	−1.55048	1.28027	1.08191
0.30	1.00000	0.00000	0.00000	1.00000	−1.12123	−1.57428	1.37664	1.12118
0.40	1.00000	0.00000	0.00000	1.00000	−1.15968	−1.59770	1.47172	1.15963
0.50	1.00000	0.00000	0.00000	1.00000	−1.19756	−1.62108	1.56568	1.19748
0.60	1.00000	0.00000	0.00000	1.00000	−1.23490	−1.64438	1.65859	1.23483
0.70	1.00000	0.00000	0.00000	1.00000	−1.27199	−1.66797	1.75067	1.27189
0.80	1.00000	0.00000	0.00000	1.00000	−1.30922	−1.69208	1.84234	1.30915
0.90	1.00000	0.00000	0.00000	1.00000	−1.34678	−1.71709	1.93364	1.34669
1.00	1.00000	0.00000	0.00000	1.00000	−1.38510	−1.74316	2.02515	1.38496
1.10	1.00000	0.00000	0.00000	1.00000	−1.42472	−1.77088	2.11736	1.42457
1.20	1.00000	0.00000	0.00000	1.00000	−1.46640	−1.80061	2.21136	1.46623
1.30	1.00000	0.00000	0.00000	1.00000	−1.51100	−1.83307	2.30797	1.51072
1.40	1.00000	0.00000	0.00000	1.00000	−1.55913	−1.86853	2.41837	1.56881
1.50	1.00000	0.00000	0.00000	1.00000	−1.61246	−1.90808	2.51488	1.61224
1.60	1.00000	0.00000	0.00000	1.00000	−1.67204	−1.95206	2.62911	1.67169
1.70	1.00000	0.00000	0.00000	1.00000	−1.74021	−2.00182	2.75555	1.74010
1.80	1.00000	0.00000	0.00000	1.00000	−1.81851	−2.05791	2.89636	1.81822
1.90	1.00000	0.00000	0.00000	1.00000	−1.91035	−2.12190	3.05858	1.91000
2.00	1.00000	0.00000	0.00000	1.00000	−2.01870	−2.19469	3.24874	2.01813
2.20	1.00000	0.00000	0.00000	1.00000	−2.30529	−2.37501	3.75800	2.30421
2.40	1.00000	0.00000	0.00000	1.00000	−2.72633	−2.61420	4.55036	2.72609
2.60	1.00000	0.00000	0.00000	1.00000	−3.37807	−2.93947	5.89616	3.37619
2.80	1.00000	0.00000	0.00000	1.00000	−4.41634	−3.38854	8.34326	4.41593
3.00	1.00000	0.00000	0.00000	1.00000	−6.19144	−4.03441	13.26690	6.19016
3.50	1.00000	0.00000	0.00000	1.00000	−24.13768	−7.97444	97.18629	23.94553
4.00	1.00000	0.00000	0.00000	1.00000	——	——	——	——

Substituting the values of the 16 coefficients from Tables 3 and 4 into Equations (24) and (25), it can obtain the intermediate variables $\overline{y_1}$ and $\overline{\varphi_1}$ in Section 1. Bringing $\overline{y_1}$ and $\overline{\varphi_1}$ into the geometric condition, Equation (21) yields intermediate variables $\overline{y_2}$ and $\overline{\varphi_2}$ at Section 2. Then, bringing the above intermediate variables $\overline{y_1}$ and $\overline{\varphi_1}$ into Equations (19) and (20), respectively, the pile displacement and internal force response of the upper and lower piles can be obtained, which is the expression of the overall pile response of the mechanically connected pile with fixed constraints at the pile bottom.

3. Finite Element Model Calculation

There are two commonly used finite element simulation modelling approaches for pile-soil interaction. One is to build a pile-soil model based on the actual situation of pile-soil interaction after simplification and assumptions. The other is to model pile springs from elastic foundation beams, using springs and damping to replace the soil around the pile. The two models have their own focus and are widely used in engineering practice. Using ABAQUS software, the pile-soil model is chosen to simulate the actual situation in

the project in order to better simulate the constitutive model of the soil and the interaction between the soil and the pile body.

3.1. Basic Parameters

The relevant design parameters for the test pile are selected from the reference [21]. The numerical analysis model is established based on the test results in the reference [21]. The length of the test pile in is 18 m, of which the pile in-ground length is 17 m, and the free section length is 1 m. The pile diameter is 0.6 m. The top of the pile can be rotated freely. Nine HRB400 steel bars are used for longitudinal reinforcement. The stirrup is an HPB235 steel bar with a diameter of 12 mm and a spacing of 200 mm. The concrete strength of the pile is C30. The cover concrete thickness of the pile is 50 mm. In the area of the test pile, there are three layers of groundwater, including the stagnant water layer, upper pressurised water layer and lower pressurised water layer, and the groundwater level is located in the range of 1–2.5 m below the ground surface. The test adopts a unidirectional multi-cycle loading mode, and the maximum load of the test is 150 kN, which is divided into 10 levels for loading. The loading load of each level is 15 kN. The load loading point was 1 m from the ground, and the test pile was buried in a non-rocky foundation. According to the test result, the total displacement of the top of the pile under the maximum load of the test was 5.06 mm, and the angle of rotation was 0.18°. The physical-mechanical parameters of the soil layers are listed in Table 5. The mechanical parameters of the piles and reinforcement are listed in Table 6.

Table 5. Physical-mechanical parameters of the soil layer.

Soil Layer	*T* (m)	*D* (kg/m^3)	*E* (MPa)	*v*	Mohr-Coulomb Model Parameter	
					φ (°)	*C* (kPa)
Fill soil	1.90	2000.00	16.00	0.30	24.00	7.00
Pulverized soil	9.20	2040.00	18.00	0.23	26.00	16.00
Sandy soil1	2.20	2060.00	50.00	0.20	34.00	0.00
Clay 1	8.50	1970.00	20.00	0.25	22.00	16.00
Sandy soil 2	3.70	2100.00	50.00	0.20	36.00	0.00
Gravel	2.40	2150.00	80.00	0.20	38.00	0.00
Clay 2	14.7	1990	20	0.25	22	16

Note: *T* is the thickness of the soil layer; *D* is the density; *E* is the modulus of elasticity; *v* is the Poisson's ratio.

Table 6. Finite element simulation of pile and reinforcement physico-mechanical parameters.

Material	*D* (kg/m^3)	*E* (MPa)	*v*	Diameter (cm)	Length (m)
Concrete pile	2400.00	30,000.00	0.20	60.00	18.00
Longitudinal reinforcement	7850.00	200,000.00	0.30	2.50	18.00
Stirrup	7850.00	200,000.00	0.30	1.00	1.53

3.2. Verification of the Correctness of the m-Method

Based on the relevant information in reference [21], ordinary piles and mechanically connected piles with different boundary conditions are established. The finite element model is established using the mechanical parameters of the test piles and reinforcement [21]. The connector is set up as a hinged support with a limit. The rotation angle limit is taken as $\varphi^0 = 1000 \times 10^{-5}$. The material constitutive models for numerical simulations are shown in Table 7. The bearing capacity problem of the pile involves pile-soil contact. There are two parts of the pile-soil contact: pile perimeter and pile bottom. The master-slave contact algorithm in face-to-face contact is chosen. The surface of the pile serves as the master face, and the face in the soil body where mutual contact with the pile occurs serves as the slave face. The face-to-face discretisation method is used for the face

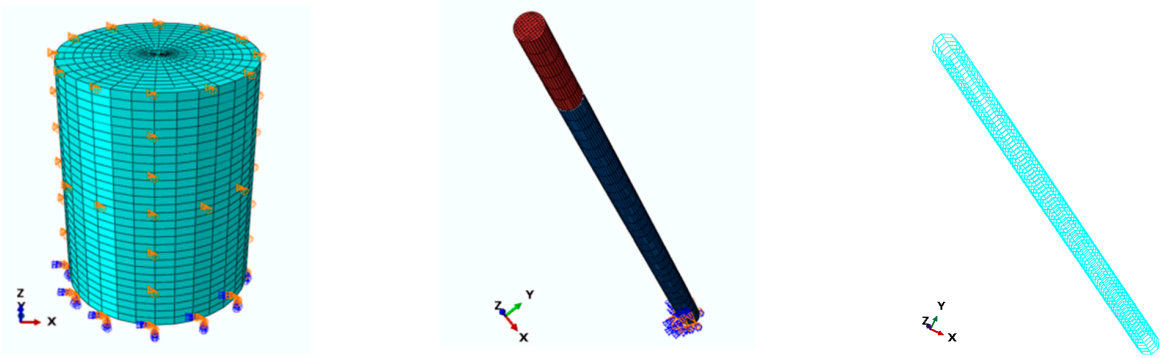
discretisation. The mechanical behaviour between the contacting faces usually consists of two components, i.e., the normal and tangential action of the contact. According to the characteristics of the model, a hard contact model is chosen for the normal action, and a penalty stiffness algorithm for the friction model is used for the tangential action. The boundary conditions at the bottom of the pile are embedded for ordinary through-length piles and mechanically connected piles.

Table 7. Finite element simulation for each material principal structure selection.

Material	Constitutive Model	Math Expression
Soil	Mohr-Coulomb model	$\tau = c - \sigma \tan \varphi$
Concrete	Ideal elastic model	E_c = 16 MPa
Reinforcement	Ideal elastic-plastic model	$\sigma_s = \begin{cases} E_s \varepsilon_s & \varepsilon_s < \varepsilon_y \\ f_y & \varepsilon_s \geq \varepsilon_y \end{cases}$
Mechanically connection	Connector	——

Note: τ is the shear strength of the soil, σ is the positive stress at a point of the soil, c is the cohesion of the soil, and φ is the angle of internal friction; E_c is the concrete modulus of elasticity; E_s is the reinforcement modulus of elasticity; σ_s is the reinforcement modulus of elasticity; f_y is the reinforcement yield strength.

The established pile-soil model is shown in Figure 5. The soil part of the model is a cylinder. The diameter of the circle is 30 m (50 times the diameter of the pile). The height of the cylinder is 38 m (2.1 times the length of the pile). Reserve pile position in the middle of the soil body. The size of the pile position is the same as the pile, and the depth of the pile position is 17 m. The dimensions and boundaries of the established pile model are the same as those of the test pile.



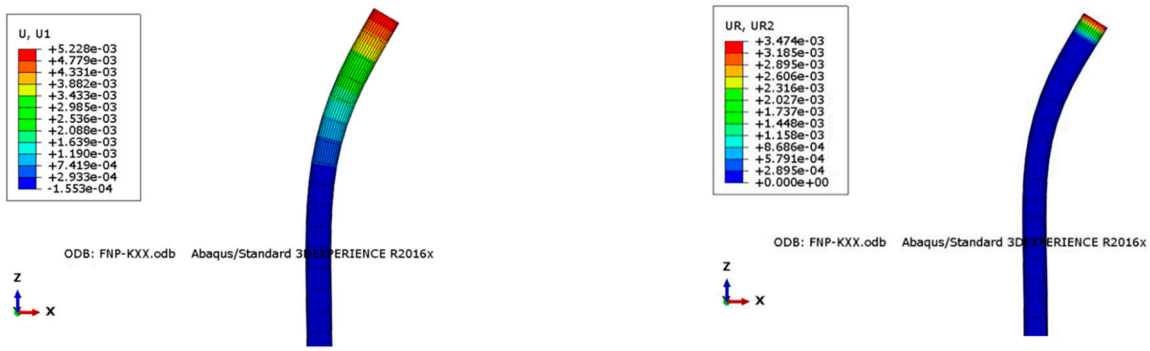
(**a**) (**b**) (**c**)

Figure 5. Mesh diagram for the finite element model. (**a**) Soil. (**b**) Foundation pile. (**c**) Reinforcing steel.

The finite element results of the test pile are shown in Figure 6. It can be seen that the simulated displacements and angles of rotation at the top of the pile are basically consistent with the test results, with the maximum displacements and angles of rotation at the pile top. Table 8 shows a comparison of the simulated and tested horizontal displacements and angles of rotation at the pile top. The relative errors of the displacements and angles of rotation are both less than 10%, indicating that the established model has good accuracy.

Table 8. A comparison of the simulated and tested horizontal displacements and angles of rotation at the pile top.

Result	Displacement (mm)		Angle of Rotation (10^{-5} r)	
	Value	Relative Error (%)	Value	Relative Error (%)
Numerical simulation	5.23	3.25	347.40	9.56
Test	5.06	0.00	314.20	0.00



(**a**) (**b**)

Figure 6. Finite element results of the test pile. (**a**) Displacements. (**b**) Angles of rotation.

3.3. Comparison of Theoretical and Numerical Simulation Results

According to the deformation coefficient of the pile $\alpha = \sqrt[5]{\frac{mb_1}{EI}} = \sqrt[5]{\frac{12.68\times10^6\times1.26}{1.5268\times10^8}} = 0.6367\ \mathrm{m}^{-1}$, it can obtain $\alpha L = 0.6367 \times 18 = 11.4606 \geq 4.0$. Combining the pile response coefficients and external load effects, the displacement and internal force responses of the embedded ordinary pile body can be obtained in Table 9.

Table 9. Displacement and internal force response of embedded ordinary pile.

z (m)z (m)	αz	y (mm)	φ (10^5r)	M (kN·mm)	Q (kN)
0.000	0.00	24.37	−639.93	0.00	400.00
0.157	0.10	22.75	−637.93	62.58	395.41
0.314	0.20	21.13	−632.00	123.77	382.50
0.471	0.30	19.54	−622.23	182.36	362.51
0.628	0.40	17.98	−608.85	237.33	336.69
0.785	0.50	16.45	−592.10	287.88	306.22
0.942	0.60	14.98	−572.29	333.34	272.21
1.099	0.70	13.55	−549.77	373.26	235.75
1.256	0.80	12.19	−524.90	407.28	197.75
1.414	0.90	10.89	−498.03	435.34	159.16
1.571	1.00	9.66	−469.60	457.31	120.75
1.728	1.10	8.51	−439.92	473.31	83.22
1.885	1.20	7.43	−409.43	483.52	47.18
2.042	1.30	6.43	−378.47	488.23	13.10
2.199	1.40	5.51	−347.38	487.76	−19.88
2.356	1.50	4.67	−316.45	482.52	−47.62
2.513	1.60	3.90	−286.02	472.96	−73.73
2.670	1.70	3.22	−256.31	459.52	−96.85
2.827	1.80	2.60	−227.57	442.70	−116.81
2.984	1.90	2.06	−199.99	422.98	−133.74
3.141	2.00	1.59	−173.76	400.84	−147.66
3.455	2.20	0.83	−125.81	351.09	−167.22
3.769	2.40	0.30	−84.51	296.80	−177.044
4.084	2.60	−0.04	−50.26	240.62	−179.22
4.398	2.80	−0.22	−23.18	184.68	−176.11
4.712	3.00	−0.29	−3.11	130.28	−170.09
5.497	3.50	−0.15	17.90	3.29	−154.53
6.282	4.00	0.00	0.00	0.00	−100.00

Figure 7 compares the theoretical and numerical simulation displacements and internal force responses of the embedded ordinary pile. It can be seen from Figure 7 that:

(1) The theoretical value of pile displacement calculated by the m-method agrees well with the numerical simulation results. The maximum displacement occurs at the

pile top. The theoretical value calculated by the m-method is 24.37 mm, while the numerical simulation value is 24.96 mm, with a relative error of 2.42%.

(2) The maximum angle of rotation of the pile occurs at the top of the pile. The theoretical maximum angle of rotation is -639.93×10^{-5} r, while the numerical simulation maximum angle of rotation is -674.67×10^{-5} r with a relative error of 5.43%.

(3) The maximum bending moment of the pile occurs at 2–4 m from the top position of the pile. The theoretical maximum value of the bending moment is 488.23 kN·m at 2.042 m depth, and the simulated maximum value of the bending moment is 460.01 kN·m at 2.50 m depth, with a relative error of 6.13%. The theoretical point of contra-flexure is at 6.28 m, and the numerical simulation point of contra-flexure is at 7.00 m.

(4) The positive shear is 400 kN at the location of the top of the pile. The theoretical maximum value of the negative shear is −179.22 kN at the depth of 4.084 m. The simulated maximum negative shear is −190.35 kN at a depth of 4.5 m, with a relative error of 6.21%. The m-method calculates the shear as zero at 2.199 m and the numerical simulation shear as zero at 2.5 m.

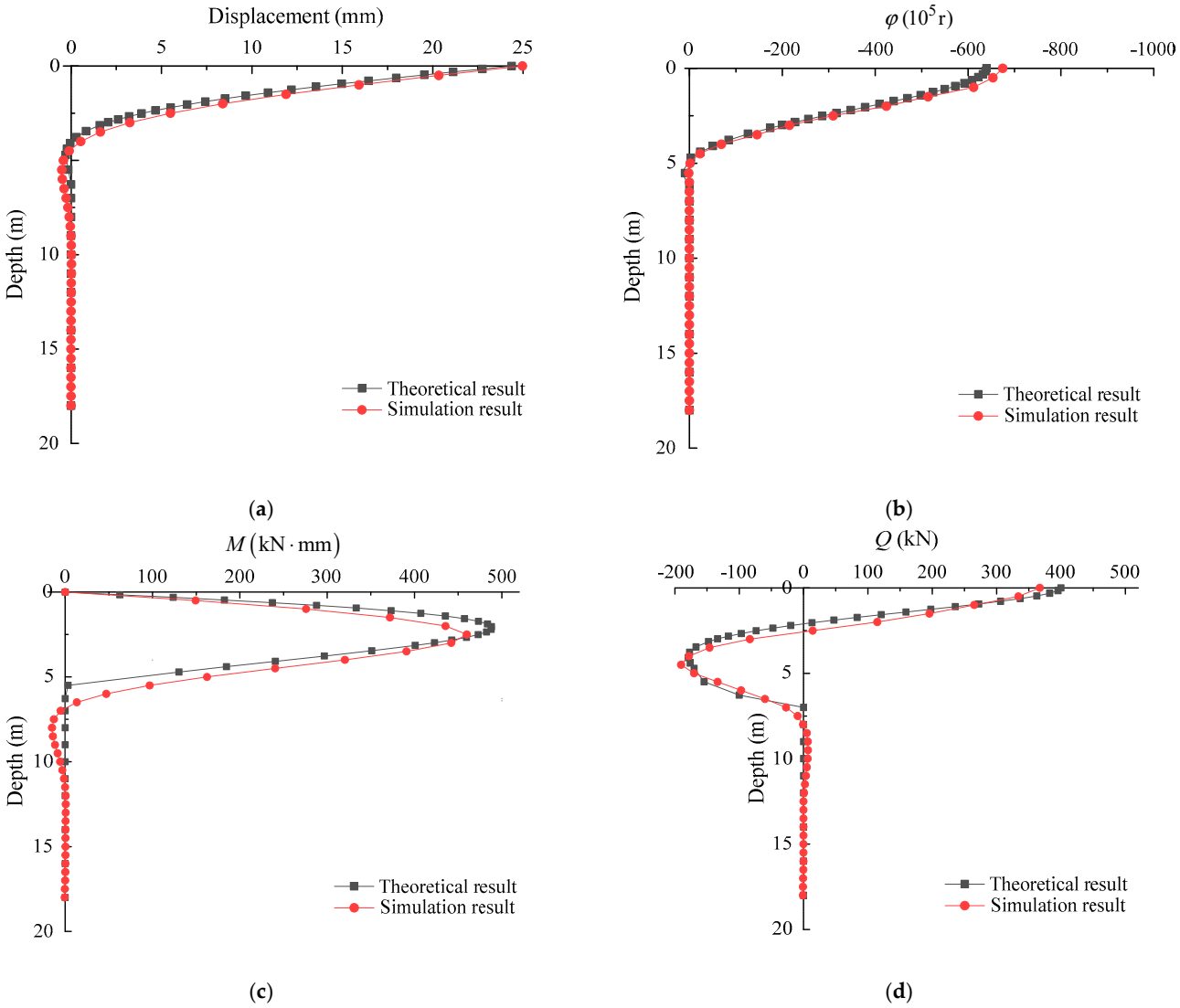


Figure 7. A comparison of theoretical and numerical simulation displacements and internal force responses of embedded ordinary pile. (**a**) Variation curve of displacement with depth. (**b**) Variation curve of the angle of rotation with depth. (**c**) Variation of shear with depth. (**d**) Variation of bending moment with depth.

According to the above analysis, it can be found that the theoretical and numerical simulation displacements and internal force responses of the embedded ordinary pile are basically consistent, which can prove the correctness of the theoretical calculation by the m-method.

Segmental calculation of embedded mechanically connected piles considering upper pile length $L_1 = 3$ m and lower pile length $L_2 = 15$ m. The deformation coefficient of the pile $\alpha_1 = \alpha_2 = \sqrt[5]{\frac{mb_1}{EI}} = \sqrt[5]{\frac{12.68\times10^6\times1.26}{1.5268\times10^8}} = 0.6367\ \mathrm{m}^{-1}$ and $\alpha_1 L_1 = 0.6367 \times 3 = 1.91$.

When, $\alpha_2 L_1 = 1.91$, the coefficients in Section 2 are $\begin{cases} \delta_{\overline{M_2}^{\Delta}\overline{y_2}^{\Delta}} = -1.91038 \\ \delta_{\overline{M_2}^{\Delta}\overline{\varphi_2}^{\Delta}} = -2.12188 \\ \delta_{\overline{Q_2}^{\Delta}\overline{y_2}^{\Delta}} = 3.05859 \\ \delta_{\overline{Q_2}^{\Delta}\overline{\varphi_2}^{\Delta}} = 1.90997 \end{cases}$.

The above coefficients are brought into Equations (17)–(20), which can be obtain:

$$\begin{cases} \delta_{\overline{y_1}^{\Delta}\overline{\varphi_0}^{\Delta}} = -0.27222 \\ \delta_{\overline{y_1}^{\Delta}\overline{M_0}^{\Delta}} = -0.04228 \\ \delta_{\overline{y_1}^{\Delta}\overline{Q_0}^{\Delta}} = 0.20291 \\ \delta_{\overline{y_1}^{\Delta}\overline{\varphi_0}^{\Delta}} = -0.63098 \\ \delta_{\overline{\varphi_1}^{\Delta}\overline{M_0}^{\Delta}} = -0.17691 \\ \delta_{\overline{\varphi_1}^{\Delta}\overline{Q_0}^{\Delta}} = -0.49999 \end{cases}.$$

When $\overline{M} = 0$, $\overline{Q} = 646.26129 \times 10^{-5}$ and $\bar{\varphi} = 1000 \times 10^{-5}$r, $\overline{y_1} = -141.08315$ and $\overline{\varphi_1} = -954.10114$. From the geometric relation, it can obtain $\overline{y_2} = \overline{y_1} = -141.08315$ and $\overline{\varphi_1} = \overline{\varphi_1} + 1000 = 45.89886 \times 10^{-5}$r. Then, the displacement and internal force response of the mechanically connected pile are obtained, as shown in Table 10.

Table 10. Displacement and internal force response of the embedded pile using mechanical connections.

z (m)z (m)	αz	y (mm)	φ (10^{-5}r)	M (kN·mm)	Q (kN)
0.0000	0.00	34.94	−1490.05	0.00	400.00
0.1570	0.10	32.60	−1486.82	62.47	393.42
0.3140	0.20	30.26	−1477.28	122.96	374.92
0.4710	0.30	27.97	−1461.67	179.71	346.30
0.6280	0.40	25.69	−1440.48	231.29	309.37
0.7850	0.50	23.449	−1414.29	276.56	265.90
0.9420	0.60	21.25	−1383.819	314.57	217.54
1.099	0.70	19.10	−1349.839	344.72	165.97
1.2560	0.80	17.01	−1313.19	366.57	112.67
1.4140	0.90	14.98	−1274.709	380.09	59.18
1.5710	1.00	13.00	−1235.30	385.26	6.89
1.7280	1.10	11.10	−1195.70	382.40	−42.87
1.8850	1.20	9.25	−1156.86	371.98	−88.88
2.0420	1.30	7.46	−1119.42	354.73	−129.95
2.1990	1.40	5.73	−1084.08	331.46	−166.81
2.3560	1.50	4.05	−1051.37	303.27	−192.86
2.5130	1.60	2.43	−1021.80	271.32	−212.56
2.6700	1.70	0.84	−995.63	236.98	−223.17
2.8270	1.80	−0.70	−973.07	201.75	−223.54
2.9840	1.90	−2.22	−954.10	167.33	−212.82
2.9840	1.90	−2.22	45.90	167.33	−212.82
3.1410	2.00	−2.13	61.43	135.22	−196.11
3.4550	2.20	−1.90	83.30	78.88	−162.69
3.7690	2.40	−1.62	94.60	32.86	−130.77
4.0840	2.60	−1.32	97.49	−3.58	−101.88

Table 10. *Cont.*

z (m)z (m)	αz	y (mm)	φ (10^{-5}r)	M (kN·mm)	Q (kN)
4.3980	2.80	−1.01	93.75	−31.64	−77.166
4.7120	3.00	−0.73	85.02	−52.62	−57.38
5.4970	3.50	−0.20	48.88	−84.74	−29.67
6.2820	4.00	0.00	0.00	−60.00	−25.04

Figure 8 compares the theoretical and numerical simulation and internal force responses of the embedded pile using mechanical connections. It can be seen from Figure 8 that:

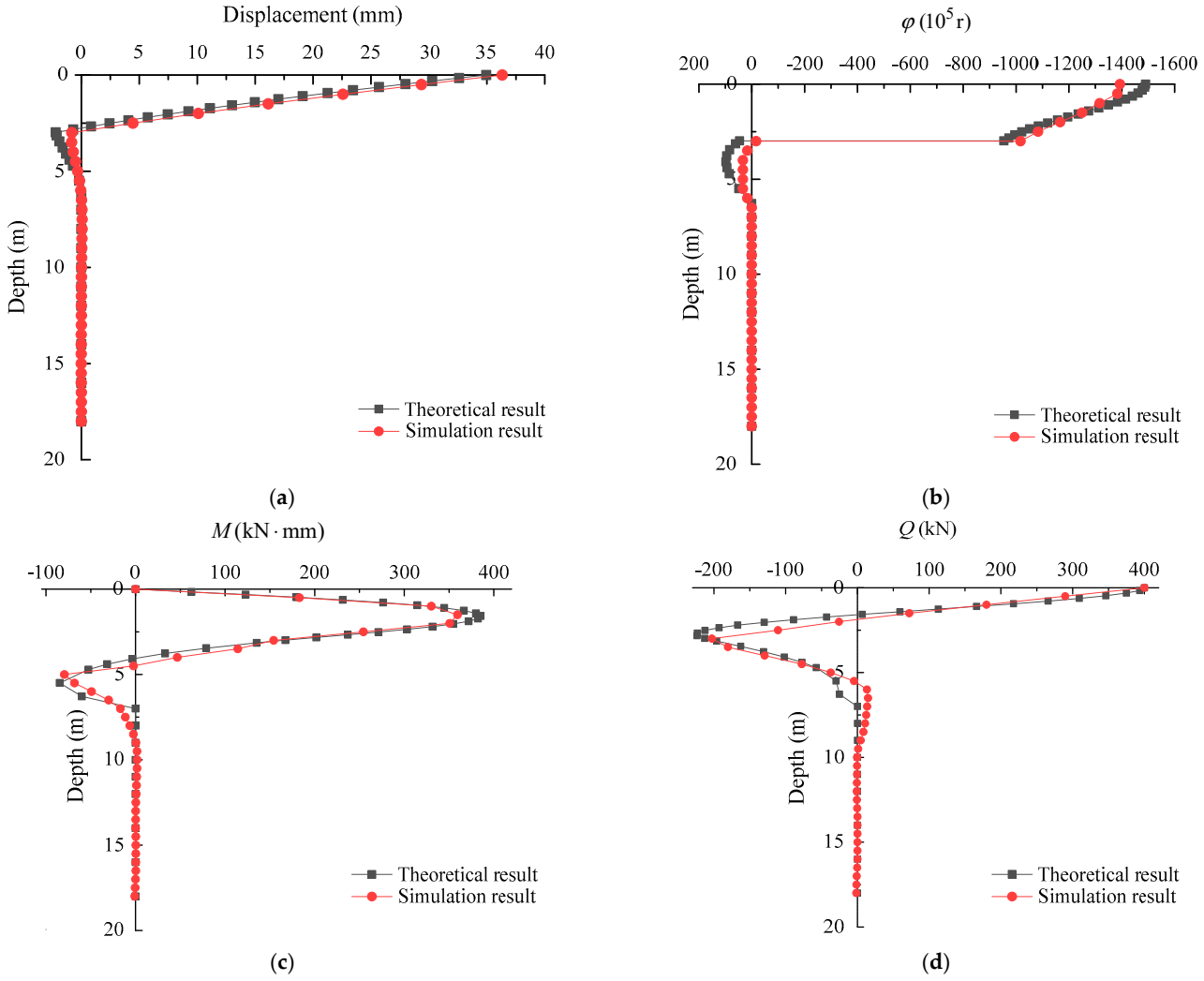


Figure 8. Comparison of theoretical and numerical simulation displacements and internal force responses of the embedded pile using mechanical connections. (**a**) Variation curve of displacement with depth. (**b**) Variation curve of the angle of rotation with depth. (**c**) Variation of shear with depth. (**d**) Variation of bending moment with depth.

(1) The theoretical and numerical simulation displacements of the mechanically connected pile fit well. The maximum displacement occurs at the top position of the pile. The theoretical maximum displacement is 34.94 mm, and the numerical simulation displacement is 36.33 mm, with a relative error of 3.83%.

(2) The maximum angle of rotation of the mechanically connected pile occurs at the top of the pile. The theoretical maximum angle of rotation is -1490.05×10^{-5} r, while the

numerical simulation maximum angle of rotation is -1393.33×10^{-5} r, with a relative error of 6.94%.

(3) The maximum positive bending moment of the mechanically connected pile occurs at 1–3 m from the top position of the pile. The theoretical maximum positive bending moment is 385.26 kN·m at 1.57 m depth, and the simulated maximum positive bending moment is 359.51 kN·m at 1.50 m depth, with a relative error of 7.16%. The theoretical maximum negative bending moment is −84.74 kN·m at 5.50 m depth, and the simulated maximum negative bending moment is −79.53 kN·m at 5.50 m depth, with a relative error of 6.55%. The theoretical point of contra-flexure is at 4.08 m, and the numerical simulation point of contra-flexure is at 4.23 m.

(4) The positive shear is 400 kN at the location of the top of the pile. The theoretical maximum value of the negative shear is −223.54 kN at a depth of 2.83 m. The simulated maximum negative shear is −203.84 kN at a depth of 4.5 m, with a relative error of 9.66%. The m-method calculates the shear as zero at 1.57 m and the numerical simulation shear as zero at 1.8 m.

According to the above analysis, it can be found that the theoretical and numerical simulation displacements and internal force responses of the embedded pile using mechanical connections are basically consistent, which can prove the correctness of the theoretical calculation by the m-method.

4. Conclusions

(1) Based on the m-method, the displacement curve equations of mechanically connected piles are established. Setting reasonable boundary conditions, the pile displacements and internal force responses of the upper and lower piles under horizontal loading are obtained, respectively, which are the expressions of the overall pile response of the mechanically connected pile.

(2) The solution method and process are expressed in the form of a table of sub-coefficients of pile internal forces, which is helpful for rapid calculation and study of the mechanically connected pile displacement and internal force response under different pile-soil conditions.

(3) The simulated displacements and angles of rotation of the pile-soil model established using ABAQUS software are basically consistent with the test results. The relative errors of the displacements and angles of rotation are both less than 10%, indicating that the established pile-soil model has good accuracy.

(4) The theoretical and numerical simulation displacements and internal forces of the mechanically connected pile fit well. The relative errors of the displacements, angles of rotation, positive and negative bending moments, and positive and negative shear forces are all less than 10%, proving the correctness of the theoretical calculation by m-method.

In summary, this study can provide effective theoretical support and methodological guidance for the displacement and internal force response of discontinuous piles.

Author Contributions: L.G. contributed to conceptualization, formal analysis, investigation and writing. M.-L.Z. contributed to methodology, funding acquisition, supervision, project administration and writing-review and editing., writing and writing-review and editing. Q.Z. contributed to formal analysis, software and data curation. G.B., X.Y. and J.D. contributed to data curation, investigation, and visualization. S.Z. and M.W. contributed to conceptualization, funding acquisition, supervision, project administration. All authors have read and agreed to the published version of the manuscript.

Funding: This research has been supported by the Natural Science Research Project of Jiangsu Province Colleges and Universities (21KJD560002 and 23KJA560007), China; Research and Innovation Team Project of Suqian College (2021TD04), China; Suqian Sci & Tech Program (H202313), China; Jiangsu Civil Architecture Society project ((2023) No. 4 Item 9), China; the Youth Fund Project of Suqian College (2023XQNA03), China; and the Fifth Provincial Research Funding Project of "333 High-level Talent Training" in 2020 (BRA2020241), China.

Data Availability Statement: The data presented in this study are available in the article here.

Conflicts of Interest: The authors declare no conflicts of interest.

List of Notations

b_0	Calculated width of the pile
EI	Flexural stiffness of the pile
E_1I_1	Flexural stiffness of the upper pile
E_2I_2	Flexural stiffness of the lower pile
L_1	Length of upper pile
L_2	Length of lower pile
M_0	External moment at the top of the upper pile
m	Proportionality coefficient of horizontal resistance factor of foundation soil with depth
Q_0	External force at the top of the upper pile
y_1	Intermediate variable
z	Pile length integral point
α_1	Horizontal deformation coefficient of the upper pile
φ_0	Displacement coefficient
φ_1	Angle of rotation at the bottom of the upper pile
δ	Displacement coefficient
$\delta_{\overline{\varphi_1}\overline{M_0}}$	Correlation coefficient between φ_1 and M_0
$\delta_{\overline{\varphi_1}\overline{Q_0}}$	Correlation coefficient between φ_1 and Q_0
$\overline{M_0}^{\Delta}$	External moment at the virtual through-length pile top
$\overline{Q_0}^{\Delta}$	External force at the virtual through-length pile top
$\overline{y_0}^{\Delta}$	Displacement at the virtual through-length pile top
$\overline{\varphi_0}^{\Delta}$	Angle of rotation at the virtual through-length pile top

References

1. Huded, P.M.; Dash, S.R. Pile foundation in alternate layered liquefiable and non-liquefiable soil deposits subjected to earthquake loading. *Earthq. Eng. Eng. Vib.* **2024**, *23*, 359–376. [CrossRef]
2. Milane, R.; Briançon, L.; Grange, S. Experimental investigation of the behaviour of pile foundations of a high-rise building. *Eur. J. Environ. Civ. Eng.* **2024**, *28*, 1394–1414. [CrossRef]
3. Lua, T.H.; Xi, X.; Tatsunori, M. Effect of pile arrangement on long-term settlement and load distribution in piled raft foundation models supported by jacked-in piles in saturated clay. *Soils Found.* **2024**, *64*, 101426.
4. Wang, J.; Jin, T.; Qin, W.; Zhang, F. Performance evaluation of post-grouting for bored piles installed in inhomogeneous gravel pebble stratum overlaid by deep and soft soil layers. *Geomech. Geoengin.* **2024**, *19*, 77–95. [CrossRef]
5. Oztürk, B. Analysis and Design of Prestressed Concrete Sheet Pile Walls. Master's Thesis, Middle East Technical University, Ankara, Turkey, 1996.
6. Chen, K.; Gan, G. Flexural Test and Numerical Simulation of a New Combination Splice for Prestressed, Precast Concrete Piles Using High-Strength Steel Strands. *Buildings* **2022**, *12*, 1371. [CrossRef]
7. Sun, C.Z.; Li, A.Q.; Miao, C.Q.; Qiao, Y. Research on cumulated damages of prestressed concrete solid pile using snap-in mechanical connection. *Earthq. Eng. Eng. Dyn.* **2018**, *38*, 211–222.
8. Sun, C.Z.; Li, A.Q.; Miao, C.Q.; Qiao, Y. Finite element analysis of mechanical properties of pile-cap connections for prestressed concrete solid pile using snap-in mechanical connection. *J. Disaster Prev. Mitig. Eng.* **2019**, *39*, 37–44.
9. Sun, C.Z.; Zhuang, M.L.; Gao, L.; Yan, J.; Yu, T.; Liu, T. Experimental study on seismic performance improvement of pile-cap joints in a prestressed concrete solid square pile using a snap-in mechanical connection. *J. Earthq. Eng.* **2023**, *27*, 3180–3201. [CrossRef]
10. Karayannis, C.G.; Chalioris, C.E. Strength of prestressed concrete beams in torsion. *Struct. Eng. Mech.* **2000**, *10*, 165–180. [CrossRef]
11. Qi, J.L.; Zhou, P.H.; Yang, X.L.; Zhou, Z.D. Application of mechanical-connection bamboo joint piles in the coastal soft soil foundation. *Build. Struct.* **2013**, *44*, 73–76.
12. Liu, L.; Xiao, L.; Li, X.Y.; Zhang, G.Z.; Wang, N.B.; Zhao, L.T. Mechanical behaviours of large-diameter rock-socketed piles under horizontal loads. *China Civ. Eng. J.* **2023**, *56*, 44–49.
13. Li, S.; Yin, J.; Zhou, J.; Yang, W. Investigation of pile-soil interaction mechanism of end-bearing foundation piles. *J. Rock Mech. Eng.* **2004**, *23*, 996–1000.
14. Yu, W.; Wu, D. Study on the joist stress of pile-supported retaining wall based on Winkler's elastic foundation beam model. *J. Zhejiang Sci-Tech Univ. Nat. Sci. Ed.* **2020**, *43*, 109–114.

15. Liu, S.; Hou, S.; Cai, Z. Lateral load test on single pile lateral bearing capacity of single pile m-method. *Chin. J. Geotech. Eng.* **2013**, *35*, 721–724.
16. Jiang, X.; Peng, R. The program development of pile foundation analysis based on m-method. *J. China Foreign Highw.* **2016**, *36*, 173–175.
17. Zhu, J.; Sun, L. Verification of m-method for Determination of Load on Piles in Soft-clay Ground. *J. Tongji Univ.* **2003**, *31*, 902–905.
18. Mao, J.; Xu, J.; Yang, L. An improved method for stabilising pile by using m-method model to the whole pile. *Rock Soil Mech.* **2018**, *39*, 1197–1202.
19. *JTG 3363–2019*; Specifications for Design of Foundation of Highway Bridges and Culverts. People's Transportation Press: Beijing, China, 2019.
20. García, F.J.A.; da Cunha, R.P.; de Albuquerque, P.J.R.; de Farias, M.M.; Bernardes, H.C. Experimental and Numerical Behavior of Horizontally Loaded Piled Rafts with a Defective Pile. *Geotech. Geol. Eng.* **2023**, *41*, 429–439. [CrossRef]
21. Chen, X.; Sun, J.; Cai, X. Horizontal static loading test and analyses of internal force and distortion on single pile. *Rock Soil Mech.* **2010**, *31*, 753–759.

Disclaimer/Publisher's Note: The statements, opinions and data contained in all publications are solely those of the individual author(s) and contributor(s) and not of MDPI and/or the editor(s). MDPI and/or the editor(s) disclaim responsibility for any injury to people or property resulting from any ideas, methods, instructions or products referred to in the content.